Water Ice Resources on Shallow Subsurface of Mars

Subjects: Astronomy & Astrophysics

Contributor: Naihuan Zheng , Chunyu Ding , Yan Su , Roberto Orosei

The planet Mars is the most probable among the terrestrial planets in our solar system to support human settlement or colonization in the future. The detection of water ice or liquid water on the shallow subsurface of Mars is a crucial scientific objective for both the Chinese Tianwen-1 and United States Mars 2020 missions, which were launched in 2020. Both missions were equipped with Rover-mounted ground-penetrating radar (GPR) instruments, specifically the RoPeR on the Zhurong rover and the RIMFAX radar on the Perseverance rover. The in situ radar provides unprecedented opportunities to study the distribution of shallow subsurface water ice on Mars with its unique penetrating capability. The presence of water ice on the shallow surface layers of Mars is one of the most significant indicators of habitability on the extraterrestrial planet.

Mars water ice shallow subsurface Martian-based ground-penetrating radars

1. Remote Sensing Photography

Remote sensing photography utilizes high-resolution imaging cameras onboard orbiters or rovers to capture images of the surface of Mars. This method enables direct observation of the presence or absence of landforms formed by liquid water on the planet's surface. Several typical Mars imaging cameras include the Mars Orbiting Camera (MOC) carried by the Mars Global Surveyor (MGS), which can capture images with high resolution, e.g., the captured images have a resolution of 1.5–12 m/pixel (Malin et al. [1]). MRO is equipped with several cameras, e.g., the Mars Color Imager (MARCI), the High-Resolution Imaging Science Equipment (HiRISE), and the Context Camera (CTX). The SuperCam onboard the Perseverance rover is equipped with the remote micro-imager (RMI); the RMI can distinguish the grains as small as 160 µm at a distance of 2 m from the instrument with a resolution ≤ 80 µrad (Wiens et al. [2]). The Colour and Stereo Surface Imaging System (CaSSIS) onboard ESA's Exomars Trace Gas Orbiter (TGO) can acquire surface images at a resolution of ~4.6 m/pixel, including stereo imaging and color information (Thomas et al. [3]).

Extensive remote sensing photography has enabled the acquisition of imagery of the Martian surface, such as **Figure 1**a, which depicts the Acidalia mesas captured by HiRISE. The interpretation of this image suggests similarities to the Tuya landscape on Earth, indicating the possible existence of volcano–ice interaction terrain on Mars (Martínez-Alonso et al. [4]). This observation provides evidence that the mysterious landforms on Mars have been influenced by water and ice (Martínez-Alonso et al. [4]). The Galaxias Fossae region photographed by CTX (**Figure 1**b) is interpreted as exhibiting possible ice-fall-like and ice-flow morphologies (Pedersen et al. [5]). Furthermore, by comparison of recurring slope lineae (RSL) images captured by HiRISE with surface temperature

and water vapor images at the same time at Martian solar longitude (Ls) 142.7° and Ls 348.7° (**Figure 2**), the temperature increases from 158 K to 261 K, while the water vapor increases from 0.0013 kg/m^2 to 0.0097 kg/m^2. It reinforces the possibility that the triggering mechanism of RSL requires sufficient water and temperature (Howari et al. [6]). Additionally, the orbiter of the Chinese Tianwen-1 mission is equipped with medium- and high-resolution cameras (0.5 m@265 km) for imaging of key areas where water may be present (Li et al. [7]).

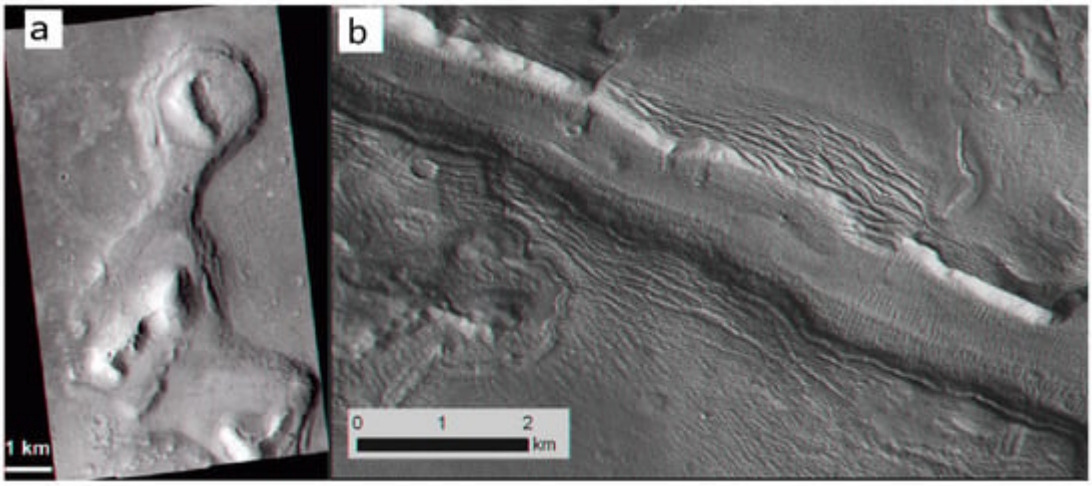

Figure 1. (**a**) The Acidalia mesas are considered to be flat-topped mountains (adapted from Martínez-Alonso et al. [4]); (**b**) an example from Galaxias Fossae (adapted from Pedersen and Head [8]).

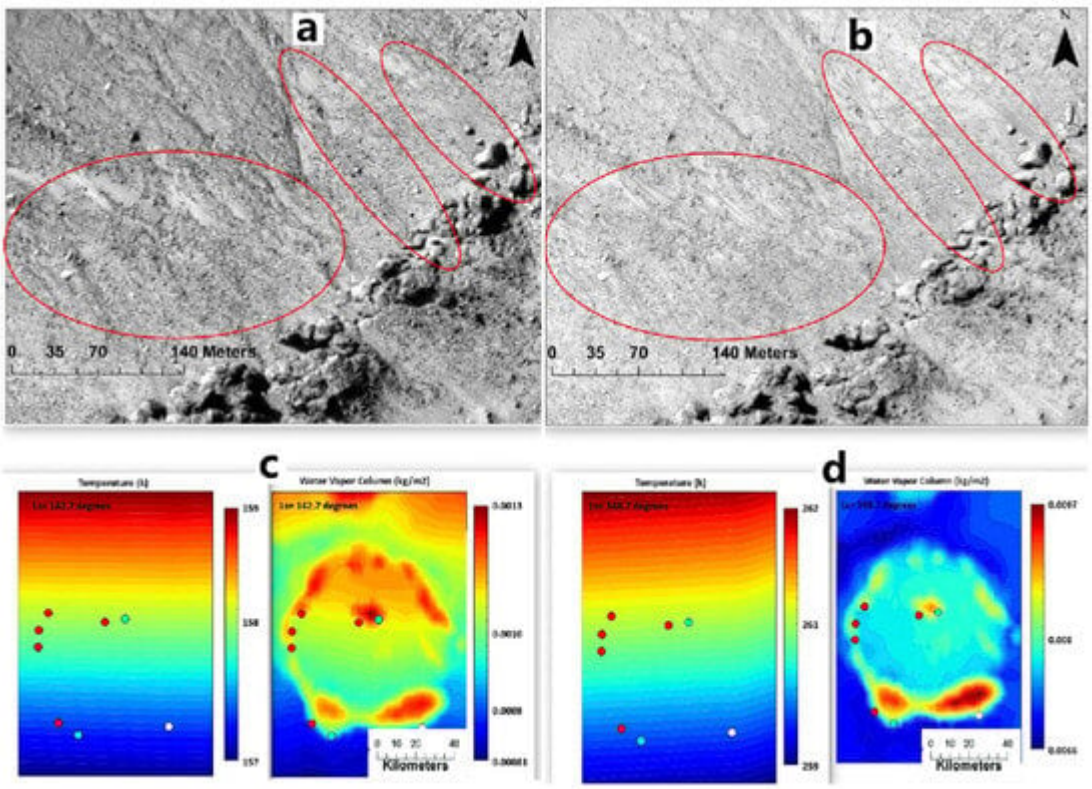

Figure 2. (**a**,**b**) display HiRISE data for Asimov crater (47°S, 5°E) at Ls 142.7° and Ls 348.7°, respectively, showcasing variations in recurring slope lineae (red circles) in the images. (**c**,**d**) depict relevant atmospheric

parameters that were captured at the same time as the HiRISE data acquisition on the Martian surface (adapted from Howari et al. [6]).

2. Radar Observation

The detection of shallow surface water ice on Mars is primarily accomplished through the use of radar equipment on orbiters or Mars rovers (Zhou et al. [9], Picardi et al. [10][11], Seu et al. [12][13], Zhou et al. [14]). The working principle of the Martian-based ground-penetrating radar can be summarized as follows (Zhou et al. [9], Qiu and Ding [15]): The radar antenna emits radar pulses towards the subsurface of Mars. When the radar electromagnetic waves encounter differences in impedance from subsurface materials, reflections and scattering of the electromagnetic waves occur at the interfaces between different materials. These echo signals are then captured by the radar antenna. The data received by the radar are then analyzed to calculate the subsurface stratification and thickness of the soil on Mars (Chen et al. [16]), as well as the dielectric properties of the subsurface material, such as the value of dielectric loss and relative permittivity. By determining the polarization of the radar signal, it is potentially feasible to ascertain the presence of water ice in the superficial layers of the detection area (Zhou et al. [14], Dong et al. [17], Liu et al. [18]). By processing these echo signals, the subsurface structure of Mars' surface and the composition of the subsurface materials can also be revealed (Grima et al. [19], Nouvel et al. [20]).

Orbiter-based radars such as MARSIS, SHARAD, and MOSIR are used to detect the global scale of Mars, with the advantage of a wide detection range. In situ ground-penetrating radars, such as RoPeR and the RIMFAX, are used for localized detection in the landing areas and have the advantage of higher precision to examine the localized subsurface structure with an unprecedented resolution compared to those of orbiter-based ground-penetrating radar.

Installed on the ESA's Mars Express space probe, the Mars Advanced Radar for Subsurface and Ionosphere Sounding (MARSIS) operates at central frequencies of 1.8, 3, 4, and 5 MHz (Picardi et al. [10][11]). With a theoretical penetration depth of 0.5–5 km, the radar is primarily used to detect the distribution of water ice beneath the Martian subsurface, local geological stratigraphy, and subsurface aquifers (Jordan et al. [21]).

Similarly, the Mars Reconnaissance Orbiter (MRO) carries shallow radar (SHARAD) with a central frequency of 20 MHz and a theoretical penetration depth of 0.1–1 km (Seu et al. [13]). SHARAD is capable of detecting stratified structures up to one kilometer below the Martian surface and is primarily used for detecting water ice, geological subsurface structure, and subsurface aquifers below the subsurface of Mars (Seu et al. [12], Xiong et al. [22]).

For instance, Bramson et al. [23] compared the time delay between surface and subsurface radar reflector from SHARAD (**Figure 3**c) with the terrace depth (**Figure 3**b) of terrace-type crater within the Arcadia Planitia determined by digital terrain models (DTMs) from HiRISE (**Figure 3**a), to work out the dielectric constant and constrain the materials' composition, and finally suggested that much of the upper region of the area is likely to be water ice. Anomalously bright subsurface reflections were identified in MARSIS radar observations collected from

May 2012 to December 2015 over Planum Australe (**Figure 4**), which were construed as due to the presence of liquid water at the bottom of the SPLDs (Orosei et al. [24]).

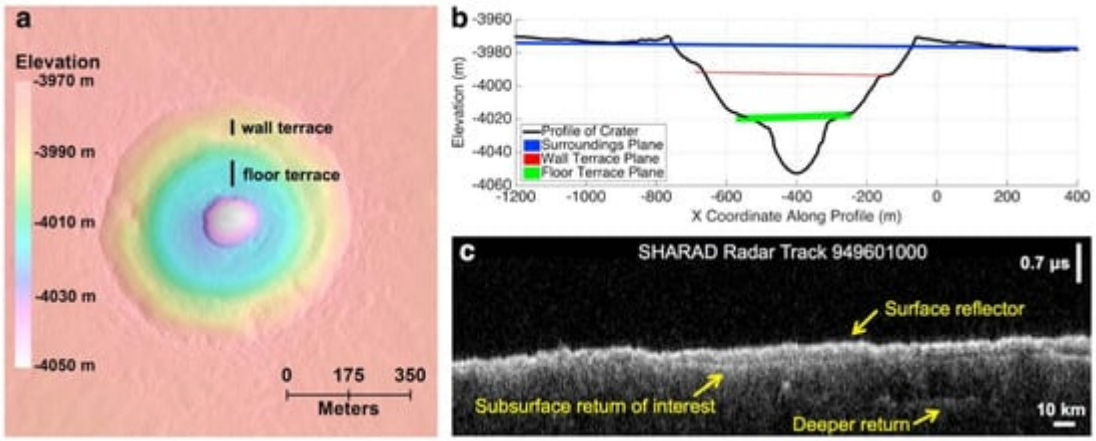

Figure 3. (**a**) DTM of the double terrace crater. (**b**) Crater profile with planes close to the surroundings and the elevation of each terrace. (**c**) SHARAD radar observations through Badger Crater. (Adapted from Bramson et al. [23]).

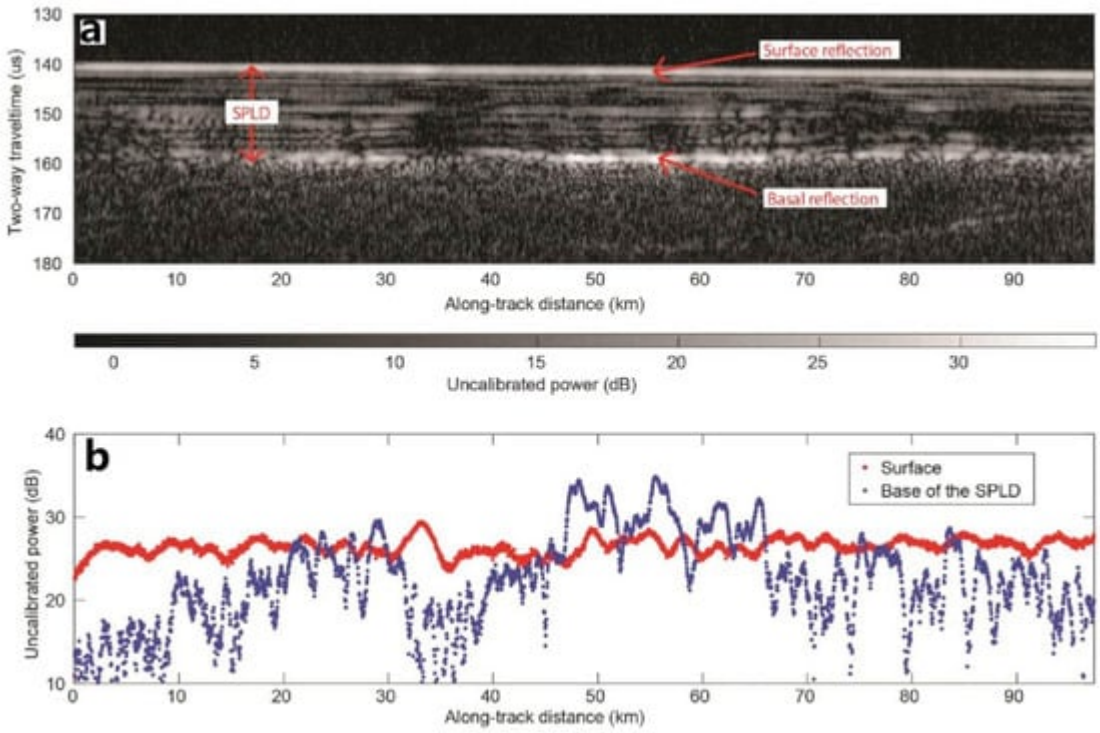

Figure 4. Radar data collected by MARSIS radar for the Planum Australe region on the southern pole of Mars. (**a**) Radargram for MARSIS orbit 10737. the bottom reflector corresponds to the South Polar Layered Deposits (SPLDs)/basal material interface. (**b**) Plot of surface and basal echo power for the radargram in (a) (adapted from Orosei et al. [24]).

China's Tianwen-1 spacecraft with MOSIR subsurface detection radar is currently exploring Mars, but the relevant detection data and research results have not yet been officially released (Li et al. [7], Fan et al. [25]). Its high-frequency mode operates at a center frequency ranging from 30 to 50 MHz, while its low-frequency mode operates at a center frequency of 10–15 MHz and 15–20 MHz (Fan et al. [25]). It has a subsurface structure penetration depth of about 100 m and an ice penetration depth of about 1000 m (Fan et al. [25]). Its thickness resolution capability is at the meter level, and it is primarily utilized for detecting water ice and subsurface structure on Mars (Li et al. [7], Hong et al. [26], Fan et al. [25]).

Martian-based ground-penetrating radars are also beginning to be deployed on the surface of Mars to reveal the secrets beneath its surface (Hamran et al. [27], Li et al. [28]). For instance, the Zhurong rover carries an in situ detection radar, RoPeR, which is a Martian-based ground-penetrating radar (Zhou et al. [9]). It operates at 15–95 MHz for the low-frequency channel and 450–2150 MHz for the high-frequency channel, with thickness resolution at the meter and centimeter levels, respectively. It can be used to detect the regions with depths of tens of meters below the Martian surface (Zhou et al. [9], Chen et al. [16], Li et al. [28]). The Perseverance rover also carries a Martian-based ground-penetrating radar, RIMFAX, primarily used to detect shallow surface geological structures and water ice on Mars [29]. Additionally, the ESA plans to carry a Martian-based ground-penetrating radar named WISDOM on board the ExoMars Rover soon (Herve et al. [30]).

3. Measurements by Gamma Ray Spectroscopy and Neutron Spectrometers

The Gamma Ray Spectrometer (GRS) onboard NASA's Mars Odyssey allows for the mapping of the chemical makeup on Mars to depths of 10 cm to 1 m below the surface through the measurement of gamma rays from space and their interactions with various surface materials (Evans et al. [31], Saunders et al. [32]). The GRS consists of the Gamma Sensor (GS), the Neutron Spectrometer (NS), and the High-Energy Neutron Detector (HEND). The neutron detector equipment like NS and HEND measures neutrons with different energy levels liberated from the near-surface of Mars by cosmic rays. It analyzes the energy reaction between neutrons and hydrogen nuclei and measures the gamma rays to obtain the content of hydrogen atoms (water and potential organic matter) in the soil at different depths, thus inferring water ice does exist on the near-surface (Saunders et al. [32]). This enables the identification of the number and type of chemical elements present, as well as the distribution of hydrogen, which can provide evidence of water ice (Evans et al. [31], Saunders et al. [32]). The GRS is capable of planet-wide mapping of hydrogen abundance on Mars at a spatial resolution of approximately 600 km, enabling inferences to be made that water ice may exist near the Martian surface (Saunders et al. [32]).

Boynton et al. [33] utilized the GRS observation to create a superthermal neutron flux map from the neutron energy spectrometer (**Figure 5**). Through this analysis, two hydrogen-rich regions near the Martian northern pole and southern pole were identified, suggesting that the source of this hydrogen in the subsurface may be ice. The globally distributed superthermal neutron flux map can be used to assist in the interpretation of whether Martian-based ground-penetrating radar detects regions of water ice.

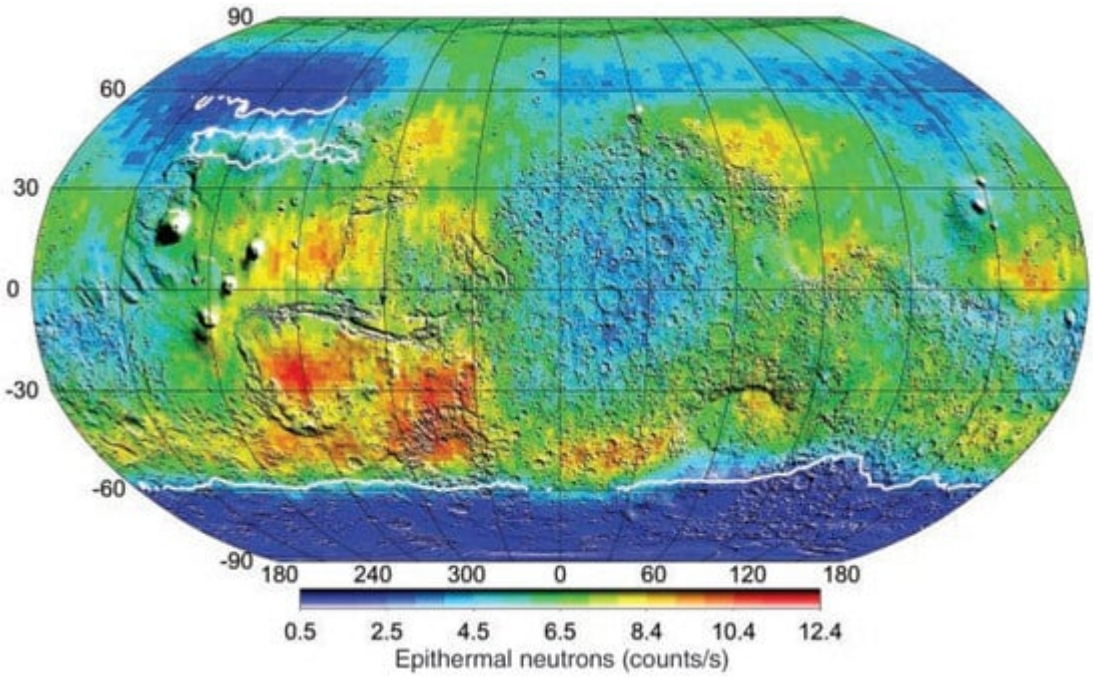

Figure 5. Super thermal neutron flux map created using data from the neutron energy spectrometer (adapted from Boynton et al. [33]).

The distribution of superthermal neutrons for 55 days at energies ranging from 0.4 eV to 100 keV plotted by HEND (**Figure 6**) suggested that the deviation of the mean and maximum neutron count rates in the northern and southern hemispheres corresponds to 5% water by weight in the homogeneous subsurface layer, with the higher content likely related to chemically bound water in the subsurface layer. The low superthermal neutron flux in the south is due to the higher water ice content within the lower subsurface layer than the upper subsurface. Under this hypothesis, Mars has large areas at low-elevation regions of the northern hemisphere and high-elevation regions of the southern hemisphere that contain the uppermost subsurface hydrogen, which may be bound in water ice. This hypothesis requires support from the global surface and subsurface water transport mechanisms on Mars (Mitrofanov et al. [34]).

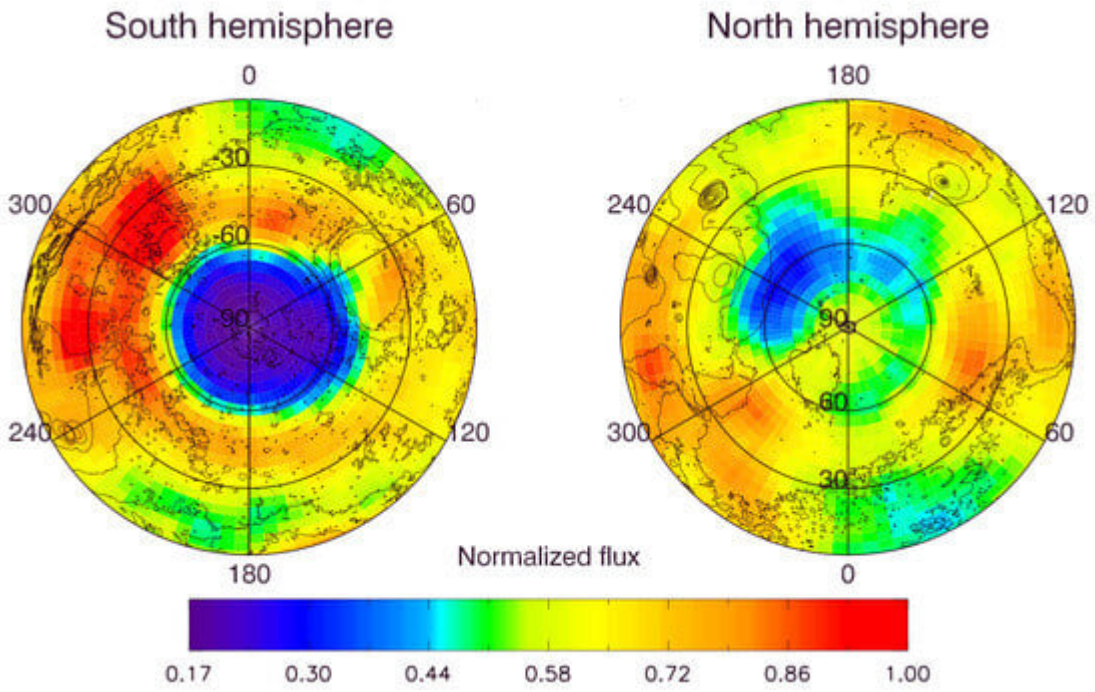

Figure 6. Initial plot of HEND measurements of Mars' superthermal neutron orbit during the first 55 days of mapping at energies ranging from 0.4 eV to 100 keV (adapted from Mitrofanov et al. [34]).

The Fine-Resolution Epithermal Neutron Detector (FREND) onboard TGO is an orbital neutron telescope, capable of detecting hydrogen on the subsurface of Mars up to 1 m depth (Mitrofanov et al. [35]). Mitrofanov et al. [36] analyzed FREND data for the Valles Marineris (VM) region and interpreted the average water-equivalent hydrogen value of Candor Chaos in the central region of VM should be 40.3 wt%. The result points to the presence of water ice permafrost or large amounts of highly hydrated minerals in the subsurface at equatorial latitudes.

The Curiosity rover is equipped with the Dynamic Albedo Detector of Neutrons (DAN), which enables the rover to characterize the soil composition at depths of 0.5–1 m and search for ice and water-bearing minerals beneath the Martian surface (Nikiforov et al. [37], Mitrofanov et al. [38]). This instrument operates by emitting a neutron beam at the surface and then measuring the speed at which the beam reflects. Water and water-bearing minerals are the only hydrogen-containing compounds detected on Mars in significant concentration (Busch and Aharonson [39]). Hydrogen atoms in the subsurface tend to slow down neutrons, and the magnitude of this slowing can indicate the presence of water or ice. Nikiforov et al. [37] proposed a method for estimating the hydrogen content equivalent to water using neutron-sensing data from the DAN instrument on the Curiosity rover and suggested the possible existence of water-containing material in the shallow subsurface of the Vera Rubin Ridge (Nikiforov et al. [37]). In situ radar electromagnetic sounding is also sensitive to the water content of the subsurface, which affects the penetration depth of radar electromagnetic waves. Therefore, this technique can provide important information for other regions of Mars where in situ radar sounding is performed to study the Martian subsurface.

4. Soil Analysis

The lander and rover missions were able to analyze the water-ice content of the exploration areas by collecting soil samples or by conducting a direct analysis of soil composition. For example, the Phoenix lander landed in the permafrost zone of the Martian surface and subsequently explored the subsurface ice by collecting soil samples (Smith et al. [40]). Excavations at the landing site revealed the presence of white material beneath the ground (**Figure 7**), which provides evidence for the presence of liquid brine on Mars (Rennó et al. [41]). The Zhurong rover, equipped with the Mars Surface Composition Explorer, is expected to discover indications of water ice in the Utopian Plainita by directly analyzing the composition of materials in the soil (Li et al. [7]).

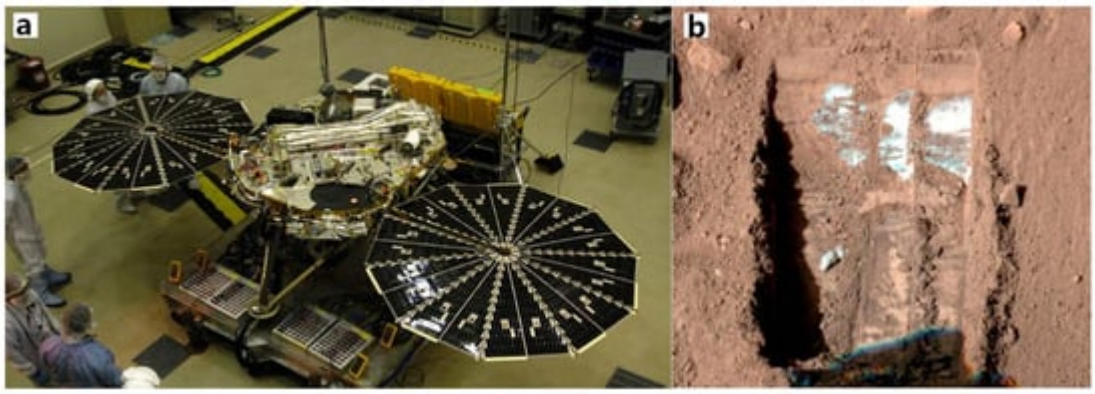

Figure 7. (**a**) Image of the Phoenix lander during the testing phase (adapted from Smith et al. [40]), and (**b**) an image showing the Phoenix robotic arm positioned to excavate the Martian surface. The white area in the image indicates the location of the water ice (adapted from Rennó et al. [41]).

5. Other Observation Methods

The widespread presence of clay, rounded gravels, salt patches at lower elevations, and hydrates containing iron compounds, as well as the occurrence of small channels on Mars, all provide evidence of past water flow on the planet (Bibring et al. [42]). The specific minerals found in Martian rocks provide insight into the previous environmental conditions that existed on the planet, including those suitable for life. For instance, the presence of sulfates and water-bearing carbonates in certain Martian meteorites, known as basaltic snow crystals, suggests that they were in an environment containing liquid water before being ejected (Nazari-Sharabian et al. [43]).

The recurring slope lineae (RSL) that form on present-day Mars are characterized by low albedo and are believed to be the result of transient liquid water flow (Stillman et al. [44]). Different parts of Mars produce RSL through various mechanisms, and all slopes containing RSL display evidence of hydrated salts, as shown in **Figure 8**. Moreover, warm slopes in the Martian seasons can produce liquid water in contemporary Mars (Ojha et al. [45]). Subsequently, through spectral data obtained from OMEGA (Observatoire pour la Mineralogie, l'Eau, la Glace et l'Activite), two forms of water presence on Mars have been identified. They are extensive water ice deposits in the polar regions of Mars and water-containing minerals on the Martian surface, respectively (Bibring et al. [42]). Analysis of near-infrared data from CRISM (Compact Reconnaissance Imaging Spectrometer for Mars) and OMEGA has revealed a widespread distribution of water-bearing minerals on Mars. Specifically, hydrous silicates

are primarily distributed in the south highlands, while water-bearing minerals in the northern lowlands exhibit greater compositional diversity and are found in various geological epochs (Bibring et al. [42]). This indicates that the forms of water present on Mars are highly diverse and span multiple geological eras.

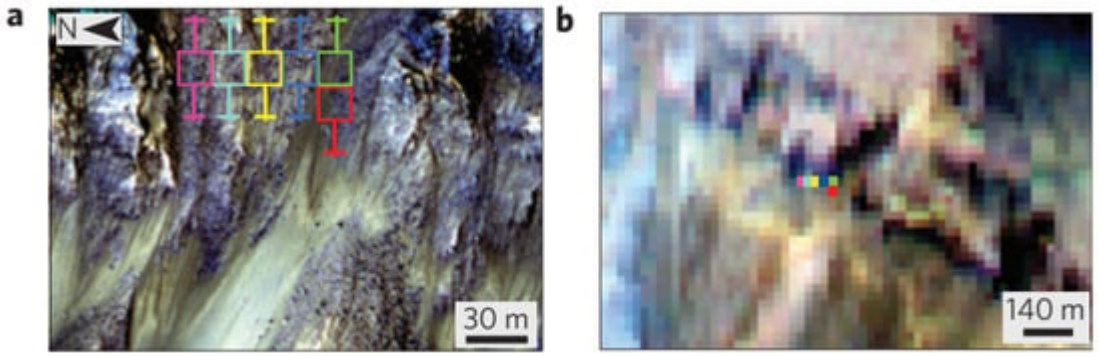

Figure 8. Recurring slope lineae in Palikir Crater (adapted from Ojha et al. [45]). (**a**) Infrared images of RSL on the slope of Palikir Crater. Colored boxes indicate the uncertainty of CRISM pixel locations; (**b**) synchronized CRISM observations.

In mineralogical surveys, it has been found that water-bearing minerals on Mars are mainly composed of Fe/Mg smectites, chlorite, and hydrated silica (Carter et al. [46]). Most of these water-bearing minerals formed before the middle of the Noachian, with a smaller portion continuing to form into the Hesperian and early Amazonian. Subsequent analysis, through crater age dating, has revealed that water-bearing minerals predominantly formed during the Noachian and the early period of Hesperian. The formation of these minerals decreased during the late Hesperian and Amazonian. Analysis of water-bearing minerals within impact melt materials inside craters has confirmed the presence of groundwater or previously existing hydrated minerals, subsurface ice, and impactor ice throughout Mars' history (Sun and Milliken [47], Wernicke and Jakosky [48]).

Based on estimations of the global water content on Mars, the water stored in and required for the formation of water-bearing minerals is estimated to range from 130–260 m of Global Equivalent Layer (GEL), with a theoretical range of 70–860 m GEL (Wernicke and Jakosky [48]). The estimated global water equivalent on Mars falls between 173–317 GEL, with a potential range of 110–1114 m GEL (Wernicke and Jakosky [48]). This underscores the significance of water-bearing minerals as a crucial reservoir of water on Mars, providing valuable insights for future endeavors in detecting water ice reserves and extracting water resources on the planet Mars.

References

1. Malin, M.; Danielson, G.; Ravine, M.; Soulanille, T. Design and development of the Mars Observer Camera. Int. J. Imaging Syst. Technol. 1991, 3, 76–91.
2. Wiens, R.C.; Maurice, S.; Robinson, S.H.; Nelson, A.E.; Cais, P.; Bernardi, P.; Newell, R.T.; Clegg, S.; Sharma, S.K.; Storms, S.; et al. The SuperCam Instrument Suite on the NASA Mars 2020

Rover: Body Unit and Combined System Tests. Space Sci. Rev. 2020, 217, 4.

3. Thomas, N.; Cremonese, G.; Ziethe, R.; Gerber, M.; Brändli, M.; Bruno, G.; Erismann, M.; Gambicorti, L.; Gerber, T.; Ghose, K.; et al. The Colour and Stereo Surface Imaging System (CaSSIS) for the ExoMars Trace Gas Orbiter. Space Sci. Rev. 2017, 212, 1897–1944.
4. Martínez-Alonso, S.; Mellon, M.T.; Banks, M.E.; Keszthelyi, L.P.; McEwen, A.S.; Team, T.H. Evidence of volcanic and glacial activity in Chryse and Acidalia Planitiae, Mars. Icarus 2011, 212, 597–621.
5. Pedersen, G.; Head, J., III; Wilson, L. Formation, erosion and exposure of Early Amazonian dikes, dike swarms and possible subglacial eruptions in the Elysium Rise/Utopia Basin Region, Mars. Earth Planet. Sci. Lett. 2010, 294, 424–439.
6. Howari, F.M.; Sharma, M.; Xavier, C.M.; Nazzal, Y.; Alaydaroos, F. Atmospheric, Geomorphological, and Compositional Analysis of Martian Asimov and Hale Craters: Implications for Recurring Slope Lineae. Front. Astron. Space Sci. 2022, 8, 244.
7. Li, C.; Zhang, R.; Yu, D.; Dong, G.; Liu, J.; Geng, Y.; Sun, Z.; Yan, W.; Ren, X.; Su, Y.; et al. China’s Mars exploration mission and science investigation. Space Sci. Rev. 2021, 217, 57.
8. Pedersen, G.B.M.; Head, J.W. Evidence of widespread degraded Amazonian-aged ice-rich deposits in the transition between Elysium Rise and Utopia Planitia, Mars: Guidelines for the recognition of degraded ice-rich materials. Planet. Space Sci. 2010, 58, 1953–1970.
9. Zhou, B.; Shen, S.; Lu, W.; Liu, Q.; Tang, C.; Li, S.; Fang, G. The Mars rover subsurface penetrating radar onboard China’s Mars 2020 mission. Earth Planet. Phys. 2020, 4, 345–354.
10. Picardi, G.; Biccari, D.; Seu, R.; Plaut, J.; Johnson, W.; Jordan, R.; Safaeinili, A.; Gurnett, D.; Huff, R.; Orosei, R.; et al. MARSIS: Mars advanced radar for subsurface and ionosphere sounding. In Mars Express: The Scientific Payload; NASA/ADS: Cambridge, MA, USA, 2004; Volume 1240, pp. 51–69.
11. Picardi, G.; Plaut, J.J.; Biccari, D.; Bombaci, O.; Calabrese, D.; Cartacci, M.; Cicchetti, A.; Clifford, S.M.; Edenhofer, P.; Farrell, W.M.; et al. Radar soundings of the subsurface of Mars. Science 2005, 310, 1925–1928.
12. Seu, R.; Biccari, D.; Orosei, R.; Lorenzoni, L.; Phillips, R.; Marinangeli, L.; Picardi, G.; Masdea, A.; Zampolini, E. SHARAD: The MRO 2005 shallow radar. Planet. Space Sci. 2004, 52, 157–166.
13. Seu, R.; Phillips, R.J.; Biccari, D.; Orosei, R.; Masdea, A.; Picardi, G.; Safaeinili, A.; Campbell, B.A.; Plaut, J.J.; Marinangeli, L.; et al. SHARAD sounding radar on the Mars Reconnaissance Orbiter. J. Geophys. Res. Planets 2007, 112, E05S05.
14. Zhou, H.; Feng, X.; Zhou, B.; Dong, Z.; Fang, G.; Zeng, Z.; Liu, C.; Li, Y.; Lu, W. Polarized Orientation Calibration and Processing Strategies for Tianwen-1 Full-Polarimetric Mars Rover

Penetrating Radar Data. IEEE Trans. Geosci. Remote Sens. 2022, 60, 5119914.

15. Qiu, X.; Ding, C. Radar Observation of the Lava Tubes on the Moon and Mars. Remote Sens. 2023, 15, 2850.
16. Chen, R.; Zhang, L.; Xu, Y.; Liu, R.; Bugiolacchi, R.; Zhang, X.; Chen, L.; Zeng, Z.; Liu, C. Martian soil as revealed by ground-penetrating radar at the Tianwen-1 landing site. Geology 2023, 51, 315–319.
17. Dong, Z.; Feng, X.; Zhou, H.; Liu, C.; Lu, Q.; Liang, W. Assessing the effects of induced field rotation on water ice detection of Tianwen-1 full-polarimetric Mars rover penetrating radar. IEEE Trans. Geosci. Remote Sens. 2021, 60, 1–13.
18. Liu, H.; Li, J.; Meng, X.; Zhou, B.; Fang, G.; Spencer, B.F. Discrimination Between Dry and Water Ices by Full Polarimetric Radar: Implications for China's First Martian Exploration. IEEE Trans. Geosci. Remote Sens. 2022, 61, 5100111.
19. Grima, C.; Kofman, W.; Herique, A.; Orosei, R.; Seu, R. Quantitative analysis of Mars surface radar reflectivity at 20 MHz. Icarus 2012, 220, 84–99.
20. Nouvel, J.F.; Herique, A.; Kofman, W.; Safaeinili, A. Radar signal simulation: Surface modeling with the facet method. Radio Sci. 2004, 39, RS1013.
21. Jordan, R.; Picardi, G.; Plaut, J.; Wheeler, K.; Kirchner, D.; Safaeinili, A.; Johnson, W.; Seu, R.; Calabrese, D.; Zampolini, E.; et al. The Mars express MARSIS sounder instrument. Planet. Space Sci. 2009, 57, 1975–1986.
22. Xiong, S.; Muller, J.P.; Tao, Y.; Ding, C.; Zhang, B.; Li, Q. Combination of MRO SHARAD and deep-learning-based DTM to search for subsurface features in Oxia Planum, Mars. Astron. Astrophys. 2023, 676, A16.
23. Bramson, A.M.; Byrne, S.; Putzig, N.E.; Sutton, S.; Plaut, J.J.; Brothers, T.C.; Holt, J.W. Widespread excess ice in arcadia planitia, Mars. Geophys. Res. Lett. 2015, 42, 6566–6574.
24. Orosei, R.; Lauro, S.E.; Pettinelli, E.; Cicchetti, A.; Coradini, M.; Cosciotti, B.; Di Paolo, F.; Flamini, E.; Mattei, E.; Pajola, M.; et al. Radar evidence of subglacial liquid water on Mars. Science 2018, 361, 490–493.
25. Fan, M.; Lyu, P.; Su, Y.; Du, K.; Zhang, Q.; Zhang, Z.; Dai, S.; Hong, T. The Mars orbiter subsurface investigation radar (MOSIR) on China's Tianwen-1 mission. Space Sci. Rev. 2021, 217, 8.
26. Hong, T.; Su, Y.; Fan, M.; Dai, S.; Lv, P.; Ding, C.; Zhang, Z.; Wang, R.; Liu, C.; Du, W.; et al. Flight Experiment Validation of Altitude Measurement Performance of MOSIR on Tianwen-1 Orbiter. Remote Sens. 2021, 13, 5049.

27. Hamran, S.E.; Paige, D.A.; Allwood, A.; Amundsen, H.E.; Berger, T.; Brovoll, S.; Carter, L.; Casademont, T.M.; Damsgård, L.; Dypvik, H.; et al. Ground penetrating radar observations of subsurface structures in the floor of Jezero crater, Mars. Sci. Adv. 2022, 8, eabp8564.
28. Li, C.; Zheng, Y.; Wang, X.; Zhang, J.; Wang, Y.; Chen, L.; Zhang, L.; Zhao, P.; Liu, Y.; Lv, W.; et al. Layered subsurface in Utopia Basin of Mars revealed by Zhurong rover radar. Nature 2022, 610, 308–312.
29. Farley, K.A.; Williford, K.H.; Stack, K.M.; Bhartia, R.; Chen, A.; de la Torre, M.; Hand, K.; Goreva, Y.; Herd, C.D.; Hueso, R.; et al. Mars 2020 mission overview. Space Sci. Rev. 2020, 216, 1–41.
30. Herve, Y.; Ciarletti, V.; Le Gall, A.; Corbel, C.; Hassen-Khodja, R.; Benedix, W.; Plettemeier, D.; Humeau, O.; Vieau, A.J.; Lustrement, B.; et al. The WISDOM radar on board the ExoMars 2022 Rover: Characterization and calibration of the flight model. Planet. Space Sci. 2020, 189, 104939.
31. Evans, L.G.; Reedy, R.C.; Starr, R.D.; Kerry, K.E.; Boynton, W.V. Analysis of gamma ray spectra measured by Mars Odyssey. J. Geophys. Res. Planets 2006, 111, E03S04.
32. Saunders, R.; Arvidson, R.; Badhwar, G.; Boynton, W.; Christensen, P.; Cucinotta, F.; Feldman, W.; Gibbs, R.; Kloss, C.; Landano, M.; et al. 2001 Mars Odyssey mission summary. Space Sci. Rev. 2004, 110, 1–36.
33. Boynton, W.; Feldman, W.; Squyres, S.; Prettyman, T.; Bruckner, J.; Evans, L.; Reedy, R.; Starr, R.; Arnold, J.; Drake, D.; et al. Distribution of hydrogen in the near surface of Mars: Evidence for subsurface ice deposits. Science 2002, 297, 81–85.
34. Mitrofanov, I.; Anfimov, D.; Kozyrev, A.; Litvak, M.; Sanin, A.; Tret'Yakov, V.; Krylov, A.; Shvetsov, V.; Boynton, W.V.; Shinohara, C.; et al. Maps of subsurface hydrogen from the high energy neutron detector, Mars Odyssey. Science 2002, 297, 78–81.
35. Mitrofanov, I.; Malakhov, A.; Bakhtin, B.; Golovin, D.; Kozyrev, A.; Litvak, M.; Mokrousov, M.; Sanin, A.; Tretyakov, V.; Vostrukhin, A.; et al. Fine Resolution Epithermal Neutron Detector (FREND) Onboard the ExoMars Trace Gas Orbiter. Space Sci. Rev. 2018, 214, 86.
36. Mitrofanov, I.; Malakhov, A.; Djachkova, M.; Golovin, D.; Litvak, M.; Mokrousov, M.; Sanin, A.; Svedhem, H.; Zelenyi, L. The evidence for unusually high hydrogen abundances in the central part of Valles Marineris on Mars. Icarus 2022, 374, 114805.
37. Nikiforov, S.; Mitrofanov, I.; Litvak, M.; Lisov, D.; Djachkova, M.; Jun, I.; Tate, C.; Sanin, A. Assessment of water content in martian subsurface along the traverse of the Curiosity rover based on passive measurements of the DAN instrument. Icarus 2020, 346, 113818.
38. Mitrofanov, I.G.; Litvak, M.L.; Varenikov, A.B.; Barmakov, Y.N.; Behar, A.; Bobrovnitsky, Y.I.; Bogolubov, E.P.; Boynton, W.V.; Harshman, K.; Kan, E.; et al. Dynamic Albedo of Neutrons (DAN) Experiment Onboard NASA's Mars Science Laboratory. Space Sci. Rev. 2012, 170, 559–582.

39. Busch, M.W.; Aharonson, O. Measuring subsurface water distribution using the Dynamic Albedo of Neutrons instrument on Mars Science Laboratory. Nucl. Instrum. Methods Phys. Res. Sect. A Accel. Spectrometers Detect. Assoc. Equip. 2008, 592, 393–399.
40. Smith, P.; Tamppari, L.; Arvidson, R.; Bass, D.; Blaney, D.; Boynton, W.; Carswell, A.; Catling, D.; Clark, B.; Duck, T.; et al. Introduction to special section on the phoenix mission: Landing site characterization experiments, mission overviews, and expected science. J. Geophys. Res. Planets 2008, 113, E00A18.
41. Rennó, N.O.; Bos, B.J.; Catling, D.; Clark, B.C.; Drube, L.; Fisher, D.; Goetz, W.; Hviid, S.F.; Keller, H.U.; Kok, J.F.; et al. Possible physical and thermodynamical evidence for liquid water at the Phoenix landing site. J. Geophys. Res. Planets 2009, 114, E00E03.
42. Bibring, J.P.; Langevin, Y.; Gendrin, A.; Gondet, B.; Poulet, F.; Berthé, M.; Soufflot, A.; Arvidson, R.; Mangold, N.; Mustard, J.; et al. Mars surface diversity as revealed by the OMEGA/Mars Express observations. Science 2005, 307, 1576–1581.
43. Nazari-Sharabian, M.; Aghababaei, M.; Karakouzian, M.; Karami, M. Water on Mars—A literature review. Galaxies 2020, 8, 40.
44. Stillman, D.E.; Michaels, T.I.; Grimm, R.E. Characteristics of the numerous and widespread recurring slope lineae (RSL) in Valles Marineris, Mars. Icarus 2017, 285, 195–210.
45. Ojha, L.; Wilhelm, M.B.; Murchie, S.L.; McEwen, A.S.; Wray, J.J.; Hanley, J.; Massé, M.; Chojnacki, M. Spectral evidence for hydrated salts in recurring slope lineae on Mars. Nat. Geosci. 2015, 8, 829–832.
46. Carter, J.; Poulet, F.; Bibring, J.P.; Mangold, N.; Murchie, S. Hydrous minerals on Mars as seen by the CRISM and OMEGA imaging spectrometers: Updated global view. J. Geophys. Res. Planets 2013, 118, 831–858.
47. Sun, V.Z.; Milliken, R.E. Ancient and recent clay formation on Mars as revealed from a global survey of hydrous minerals in crater central peaks. J. Geophys. Res. Planets 2015, 120, 2293–2332.
48. Wernicke, L.J.; Jakosky, B.M. Martian hydrated minerals: A significant water sink. J. Geophys. Res. Planets 2021, 126, e2019JE006351.